2011

Influence of antimony trioxide nanoparticle doping on superconductivity in MgB2 Bulk

Yun Zhang
University of Wollongong, yunz@uow.edu.au

S X. Dou
University of Wollongong, shi@uow.edu.au

Influence of antimony trioxide nanoparticle doping on superconductivity in MgB_2 bulk

Yun Zhang[a] and Shi Xue Dou
Institute for Superconducting and Electronic Materials, University of Wollongong, Fairy Meadow, New South Wales 2519, Australia

(Received 9 May 2011; accepted 2 August 2011)

In this work, antimony trioxide (Sb_2O_3) has been doped into MgB_2 samples to act as an additive. The doping level varies from 2.5 to 15 wt%. The effects of Sb_2O_3 addition on the lattice parameters, critical temperature (T_c), critical current density (J_c), and upper critical field (H_{c2}) have been investigated in detail. It has been found that Sb_2O_3 doping results in a small depression in T_c. The J_c value is 2.4×10^3 A·cm^{-2} for the 2.5% Sb_2O_3-doped sample at 5 K and 8 T, which is more than two times higher than for the undoped sample. The significant J_c improvement at high fields is attributed to the H_{c2} enhancement caused by the increased disorder.

I. INTRODUCTION

As one of the most promising superconductor materials,[1] MgB_2 has been studied extensively.[2–6] On the one hand, its high critical temperature (T_c), low material cost, freedom from weak links,[5,7] and multiple energy gaps[6,8,9] have attracted considerable attention for practical applications. On the other hand, several problems exist that urgently need to be solved, such as its low upper critical field (H_{c2}) and its rapidly decreasing critical current density (J_c) under increasing magnetic field, as compared to Nb-based superconductors. Currently, from a more practical and scalable point of view, addition and substitution of nanoparticles, which cause chemical and nanostructural changes in MgB_2, seem to be an effective way to induce flux pinning centers in MgB_2, thereby improving J_c and H_{c2}.[10] However, from the point of view of substitution into the lattice, only substitution of Al on Mg sites and substitution of C on B sites have proven to be possible for higher doping levels. Other substitutions, such as those involving transition metal elements (Fe, Y, Ti, Zr) in the Mg sublattice are limited to very low concentrations. In addition, compound doping with SiC,[3,11,12] the most popular choice, and B_4C[13] is effective for enhancement of the irreversibility field (H_{irr}) and J_c under higher magnetic fields. Several types of oxide doping, such as with Y_2O_3,[14] SiO_2,[15] TiO_2,[16] CeO_2,[17] and Nd_2O_3[18] have also shown positive effects on J_c and H_{irr}.

The authors' group has noted that antimony trioxide (Sb_2O_3) has a relatively low melting point, 655 °C, which is quite close to the melting point of Mg, 650 °C. The Mg and B reaction with added Sb_2O_3 dopant could involve not only $Mg + B \rightarrow MgB_2$ but also $Mg + Sb_2O_3 \rightarrow Mg_3Sb_2 + O_2$ above 655 °C. In our recent study of the effects of atmosphere on J_c of MgB_2, the particular amount of O_2 might play a very important role. (Results will be published elsewhere.) This is another reason why metal oxides have been attracting more attention than other possible dopants. These results have particularly attracted our interest towards codoping with Sb_2O_3. So, in this article, we report on a systematic study of the effects at different doping levels of the addition of nanoparticle Sb_2O_3 to MgB_2.

II. EXPERIMENT DETAILS

MgB_2 bulks were prepared by the in-situ method. Powders of Mg (99%) and amorphous B (99%) were used in a stoichiometric ratio as starting materials. To investigate the effects of doping on MgB_2 bulks, we added Sb_2O_3 nanoparticles (90–210 nm) with a purity of 99.9%. The ratios of Sb_2O_3 to MgB_2 (hereafter termed the doping ratios) in the samples were 0, 2.5, 10, and 15 wt%. The powders were well ground and pressed with a 9 ton press into stainless steel tubes 13 mm in outer diameter and 10 mm in inner diameter. This packing process was carried out in air. All samples were heated from room temperature to the sintering temperature of 800 °C and held at that temperature for 30 min in a tube furnace under Ar atmosphere at ambient pressure. The samples were then furnace cooled to room temperature. The resultant samples with 2.5, 10, and 15 wt% Sb_2O_3 were designated Samples A, B, and C, respectively. A pure MgB_2 sample, made without dopant and by applying the same process, was also fabricated for comparison. It is defined as the reference sample. The obtained MgB_2 samples were examined by a Philips PW1730 X-ray power diffractometer (Philips, Eindhoven, Netherlands) with CuK_α radiation ($\lambda = 1.541838$ Å). The X-ray diffraction (XRD) patterns were collected over a 2θ range from 20° to 80° with a step

[a]Address all correspondence to this author.
e-mail: yunz@uow.edu.au
DOI: 10.1557/jmr.2011.255

size of 0.02°. Lattice parameter calculations and quantitative phase analysis were carried out based on the XRD patterns. Magnetic measurements of the samples were conducted in a commercial Quantum Design Physical Properties Measurement System (Quantum Design, Inc., San Diego, CA). The samples were cut into rectangular blocks for measurements. Their dimensions were accurately measured with a digital micrometer. The typical dimensions of the samples used for magnetization measurements were $0.7 \times 1.5 \times 4.5$ mm^3. The DC magnetic response was obtained in an applied low field of 1 Oe using the conventional zero-field-cooled (ZFC) and field-cooled (FC) procedures. Magnetic hysteresis loops were collected at temperatures of 5 and 20 K. The critical current density, J_c, was derived from the half-width of the magnetization difference between the descending branches (M^+) and ascending branches (M^-) of the magnetization loop, using the following critical state model formula: $J_c = k\Delta M/d$, where $k = 12w/(3w-d)$ is a geometrical factor and $\Delta M = (|M^+| + |M^-|)/2/V_{l \times w \times d}$, with l, d, and w being the sample length, thickness, and width, respectively. Resistivity measurements as a function of temperature and magnetic field were collected using a four-probe resistance technique.

III. RESULTS AND DISCUSSION

The XRD patterns for the pure reference sample and Samples A, B, and C are presented in Fig. 1. All the samples seem to be well-developed MgB_2 with MgO impurity. The relative XRD peak intensity ratio of MgO (200) to MgB_2 (101) significantly increases from the reference sample to Sample A, as shown in the inset of Fig. 1. This indicates that a large amount of MgO has been formed after doping with Sb_2O_3. As the doping ratio increases from Sample A to Sample B and Sample C, the relative XRD peak intensity ratio of MgO (200) to MgB_2 (101) remains nearly constant. Another impurity, Mg_3Sb_2, appears in Samples B and C, although it is not observable in Sample A due to the low doping level. From Sample B to Sample C, the Mg_3Sb_2 peak intensities increase compared to the MgB_2 intensities. The decomposition temperature of the dopant Sb_2O_3 is about 655 °C, which is below the sintering temperature of 800 °C in this work. For the low doping ratio samples, Mg in the doped samples reacts with the decomposed oxygen to form MgO, while the decomposed Sb is solubilized into the MgB_2. As the doping ratio increases to a certain level, the Sb solution becomes saturated. For further increased doping ratios, it seems that Mg prefers to react with Sb rather than oxygen. Therefore, the amount of Mg_3Sb_2 increases from Sample A to Sample B and Sample C, while the amount of MgO remains nearly unchanged.

The full-width at half maximum (FWHM) of the indexed peaks of the XRD patterns for all samples are shown in Table I. The most heavily doped samples exhibit

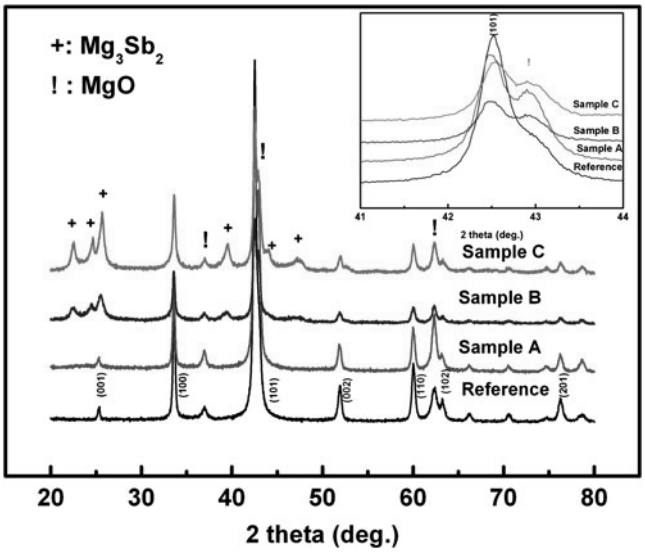

FIG. 1. X-ray diffraction patterns for the different samples. The inset shows an enlargement of the region of the main peak.

larger FWHMs than the reference sample. In general, a larger FWHM indicates a small particle size, amorphization, and large lattice parameters due to strain arising from the doping. The Rietveld refinement method was used to analyze quantitively the XRD measurements. A measure of similarity (R_{wp}) between the measured diffraction pattern and the simulated diffraction pattern is shown in Table I. A low R_{wp} indicates good agreement between the measured and simulated data. All the R_{wp} values are below 12%. This indicates that the calculated results are acceptable. The refined lattice constants along the two lattice axes (a and c) are also listed in Table I. It can be seen that compared to the reference sample, both lattice constants are decreased in the doped samples. This indicates that oxygen atoms have diffused into the lattice in the doped MgB_2. They may replace boron atoms to form $MgB_{2-x}O_x$ precipitates, leading to the reduced lattice parameters. Since the diffusion concentration of the oxygen atoms increases with the Sb_2O_3 content, the lattice parameters slightly decrease from Sample A to Sample B and Sample C.

The connectivity can be estimated by the effective cross-sectional area (A_F), defined as $A_F = \Delta\rho_{ideal}/(\rho_{300K}-\rho_{40K})$.[4] $\Delta\rho_{ideal}$ is the ideal change in resistivity from 300 to 40 K for a fully connected sample. It is set to be 7.3 μΩcm according to Ref. 19 ρ_{40K} and ρ_{300K} were obtained from the resistivity measurements. The A_Fs for all samples are listed in Table I. It can be found that the reference sample has the best connectivity, while Sample B has better connectivity than the other doped samples. Field emission scanning electron microscope (FE-SEM) images for the reference sample and Sample B are presented in Figs. 2(a) and 2(b), respectively. As can be seen from the FE-SEM images (Fig. 2), the average particle size of the 10% Sb_2O_3-doped sample is

TABLE I. Parameters and properties for all samples.

Samples	Density (mg/mm^3)	FWHM (°) (110)	FWHM (°) (002)	Lattice constants (Å) a	Lattice constants (Å) c	R_{wp} (%)
Reference	1.18	0.466	0.508	3.0853	3.5269	9.15
A (2.5%)	1.21	0.464	0.530	3.0830	3.5257	8.36
B (10%)	1.65	0.584	0.906	3.0825	3.5249	10.59
C (15%)	1.36	0.520	0.748	3.0821	3.5231	11.61
Samples	T_c (K)	J_c (5 K, 8 T) (A cm^{-2})	J_c (20 K, 0 T) (A cm^{-2})	ρ_{40k} (μΩcm)	ρ_{300k} (μΩcm)	A_F
Reference	37.7	~1.0×10^3	~2.5×10^5	64.17	123.8	0.122
A (2.5%)	36.7	~2.4×10^3	~1.7×10^5	154.42	249.63	0.077
B (10%)	36.9	~2.3×10^3	~3.6×10^5	110.7	184.94	0.098
C (15%)	36.9	~4.7×10^2	~1.4×10^5	132.88	241.02	0.067

about 40 nm, which is smaller than that of the reference sample. This clearly indicates that the particle size has been refined by Sb_2O_3 doping. Double-doping with oxygen and Sb takes place in MgB_2 with addition of Sb_2O_3. Oxygen can be incorporated within grains as precipitated nanoinclusions[20,21] or can alloy into the lattice.[22] These alloyed phases and nanoinclusions may act as nucleation centers during the formation of MgB_2 to reduce the MgB_2 grain size. The results indicate that the solubility limit of Sb in MgB_2 is between 2.5 and 10%. When the doping ratio exceeds 10 wt%, Mg_3Sb_2 impurity phase can be detected. The small amount of Mg_3Sb_2 in Sample B could enhance the grain connectivity and core density. Enhanced grain connectivity has been observed in an MgB_2 tape with a small amount of MgO impurity phase (<2.5 wt%).[23] The presence of excess Mg_3Sb phase at the grain boundaries in Sample C could result in degradation of grain connectivity.

Figure 3 shows the magnetic susceptibility (χ) against the temperature in an applied field of $H = 1$ Oe for the ZFC samples. The magnetic susceptibility for the FC condition is not displayed in the figure, since the values are very close to zero. This demonstrates that the flux pinning force in all the samples is quite large. T_c is defined as the temperature corresponding to the onset of diamagnetism. The T_c onset for the reference sample is around 37.7 K. Sample A has a T_c of 36.7 K. Samples B and C have the same T_c of 36.9 K. Compared to the reference sample, the T_c of all doped samples has decreased. The T_c decrease might be a result of increased impurity phases introduced by Sb_2O_3 doping. The transition width (ΔT_c) is defined as the temperature variation between 10 and 90% of the full drop in the magnetic susceptibility. For the reference sample, Sample A, Sample B, and Sample C, ΔT_c is 0.98, 1.38, 1.2, and 1.23 K, respectively. The small ΔT_c in the reference sample demonstrates that the defects are homogeneously distributed on the scale of the coherence length. All doped samples exhibit a higher ΔT_c than the reference sample, suggesting that the distribution of defects is more inhomogeneous.

J_c as a function of magnetic field are shown in Fig. 4. It can be seen that the J_c performance in Samples A and B shows a significant improvement over that of the reference sample under high fields at both 5 and 20 K. However, the J_c performance in Sample C has been degraded. At 5 K and 8 T, the J_c values for Samples A and B are ~2.4×10^3 and ~2.3×10^3 A·cm^{-2}, respectively, which are two times higher than for the reference sample. It is well known that grain boundary pinning is the major pinning mechanism at

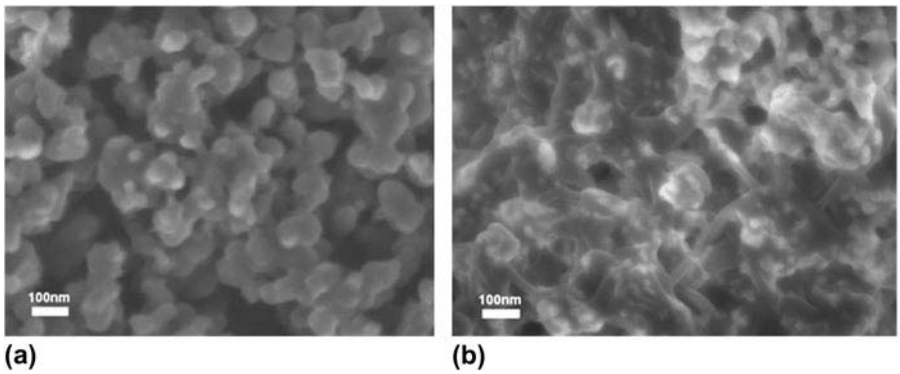

FIG. 2. Field emission scanning electron microscope images of (a) undoped and (b) 10% Sb_2O_3-doped MgB_2 samples.

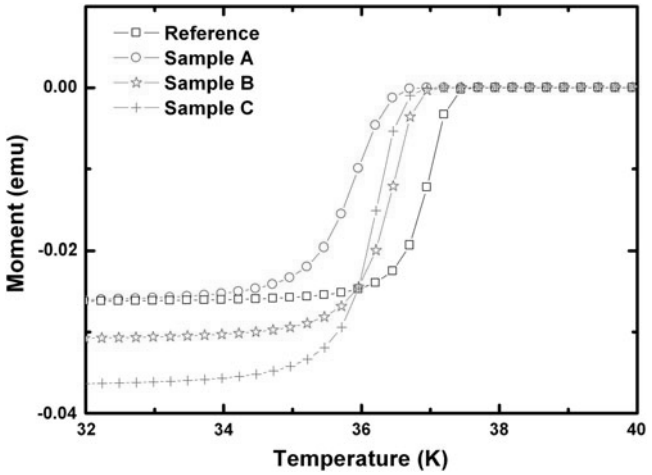

FIG. 3. Magnetic susceptibility plotted against temperature for various doping ratios.

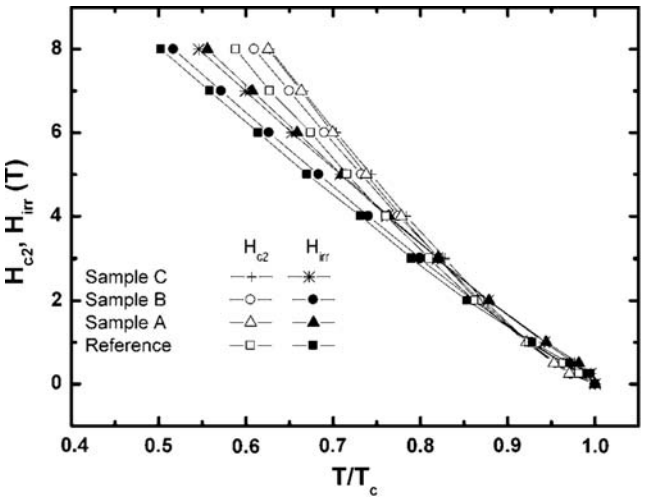

FIG. 5. Temperature dependence of H_{c2} and H_{irr}.

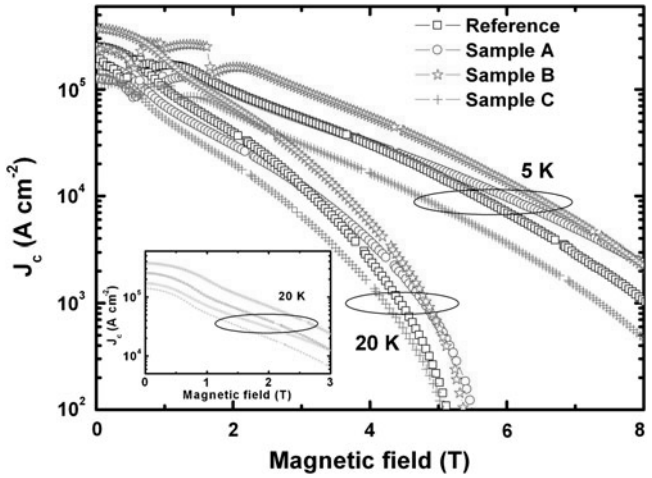

FIG. 4. Magnetic field dependence of the critical current density J_c at the temperatures of 5 and 20 K for various doping ratios. Inset: 20 K low field J_c.

high fields in MgB_2.[24] The J_c caused by the surface pinning can be estimated by $\frac{\mu_0 S_v (H_{c2}-H)^2}{4\kappa^2 H_{c2}^{1/2} H^{1/2}}$,[25] where S_v is the grain boundary surface area per unit volume, κ the Ginzburg–Landau parameter, H_{c2} the upper critical field, and H the applied field. It can be seen from this equation that J_c at high fields is predominantly determined by S_v and H_{c2}.[24] In addition, J_c is also proportional to the connectivity (A_F).[24] Therefore, higher H_{c2}, smaller grain size, and better connectivity lead to higher J_c at high fields.

The H_{irr} values at 20 K, determined by the 100 A/cm^2 criterion from Fig. 4, are 5.13, 5.51, 5.37, and 4.97 T for the reference sample and Samples A, B, and C, respectively. Since the difference between H_{c2} and H_{irr} in MgB_2 is not significant, it is expected that H_{c2} at 20 K follows the same trend. Figure 5 displays the normalized temperature dependence of the resistive H_{c2} and H_{irr}, which are obtained from the respective fields at 90 and 10% of the normal state resistivity. It can be seen that H_{c2} of the reference sample is higher than that of Sample A for $T/T_c > 0.7$. However, H_{c2} for Sample A increases faster than for the reference sample as the temperature decreases for $T/T_c < 0.7$. It is reasonable to predict that Sample A has higher H_{c2} than the reference sample at 20 K ($T/T_c \approx 0.5$). This is consistent with the H_{c2} trend observed from the magnetic field measurements, namely H_{c2} at 20 K increases from the reference sample to Sample A, and decreases from Sample A to Samples B and C. According to $H_{c2} = \Phi_0/(2\pi\mu_0\xi^2)$, where ξ is the coherence length, Φ_0 the superconducting flux quantum, and μ_0 the magnetic permeability, H_{c2} is determined by ξ. H_{c2} increases as ξ decreases. Since ξ increases with the mean free path, all the factors influencing the mean free path will change ξ and, in turn, change H_{c2}. There are two major influences that reduce the mean free path. One is lattice distortion; the other is the scattering from substituting atoms and/or diffused atoms. Oxygen atoms have been diffused into the MgB_2 lattice of Sample A due to addition of Sb_2O_3. This results in both lattice distortion and scattering. Therefore, Sample A exhibits a higher H_{c2} than the reference sample. As the content of Sb_2O_3 dopant further increases, the Mg_3Sb_2 phase appears from Sample B to Sample C, and its fraction increases from Sample B to Sample C. Since the powders of Mg and amorphous B were stoichiometrically mixed to form MgB_2, the existence of Mg_3Sb_2 indicates that there must be Mg deficiency, leading to vacancies or voids in the MgB_2. The vacancies and voids can increase the coherence length and thus reduce H_{c2} in Samples B and C.

Even though the connectivity is degraded in the doped samples (Table I), H_{c2} increases significantly from the reference sample to Sample A. The higher H_{c2} enhances the J_c performance of Sample A at high fields. In addition, the decreased grain size in Sample A, as indicated by the FWHM values in Table I, is also helpful to enhance J_c. Comparison of Sample A and Sample B shows that Sample B has a higher connectivity and a smaller grain size, but it has a lower H_{c2}. Higher connectivity and smaller grain size increase J_c, while lower H_{c2} decreases J_c. The opposite effects result in the slight change of J_c from Sample A to Sample B. Sample C has the lowest connectivity and H_{c2}, which leads to the lowest J_c at high fields.

At zero field and 20 K, J_c values of the reference sample and of Samples A, B, and C are $\sim 2.5 \times 10^5$, $\sim 1.7 \times 10^5$, $\sim 3.6 \times 10^5$, and $\sim 1.4 \times 10^5$ Acm^{-2}, respectively. The zero-field J_c of Sample B is higher than those of the other samples, while Samples A and C have lower zero-field J_c than the reference sample. The self-field J_c is proportional to the connectivity and H_{c2}. The good connectivity and higher H_{c2} in Sample B, as mentioned above, are the main reasons why the highest J_c exists in this sample.

IV. CONCLUSION

MgB_2 bulks have been fabricated with/without Sb_2O_3 doping. The effects of Sb_2O_3 doping on T_c, J_c, H_{irr}, and H_{c2} have been investigated. It has been found that Sb_2O_3 doping results in a small depression in T_c, while H_{c2} performance is improved. The best performance is shown in the 2.5% Sb_2O_3-doped sample. The reason for the enhancement of J_c is attributed to the enhancement of H_{c2}, which is caused by the increased disorder.

ACKNOWLEDGMENTS

The authors thank Dr. T. Silver, Dr. D. Attard, and Dr. X. Xu for their helpful discussions. This work was supported by the Australian Research Council, Hyper Tech Research Inc., and the University of Wollongong.

REFERENCES

1. J. Nagamatsu, N. Nakagawa, T. Muranaka, Y. Zenitani, and J. Akimitsu: Superconductivity at 39 K in magnesium diboride. *Nature* **410**, 63 (2001).
2. Y. Bugoslavsky, L.F. Cohen, G.K. Perkins, M. Polichetti, T.J. Tate, R. Gwilliam, and A.D. Caplin: Enhancement of the high-magnetic-field critical current density of superconducting MgB_2 by proton irradiation. *Nature* **411**, 561 (2001).
3. S.X. Dou, S. Soltanian, J. Horvat, X.L. Wang, S.H. Zhou, M. Ionescu, H.K. Liu, P. Munroe, and M. Tomsic: Enhancement of the critical current density and flux pinning of MgB_2 superconductor by nanoparticle SiC doping. *Appl. Phys. Lett.* **81**, 3419 (2002).
4. J.M. Rowell: The widely variable resistivity of MgB_2 samples. *Supercond. Sci. Technol.* **16**, R17 (2003).
5. D.C. Larbalestier, L.D. Cooley, M.O. Rikel, A.A. Polyanskii, J. Jiang, S. Patnaik, X.Y. Cai, D.M. Feldmann, A. Gurevich, A.A. Squitieri, M.T. Nans, C.B. Eom, E.E. Hellstrom, R.J. Cava, K.A. Regan, N. Rogado, M.A. Hayward, T. He, J.S. Slusky, P. Khalifah, K. Inumaru, and M. Haas: Strongly linked current flow in polycrystalline forms of the superconductor MgB_2. *Nature* **410**, 186 (2001).
6. S. Souma, Y. Machida, T. Sato, T. Takahashi, H. Matsui, S-C. Wang, H. Ding, A. Kaminski, J.C. Campuzano, S. Sasaki, and K. Kadowaki: The origin of multiple superconducting gaps in MgB_2. *Nature* **423**, 65 (2003).
7. M. Kambara, N.H. Babu, E.S. Sadki, J.R. Cooper, H. Minami, D.A. Cardwell, A.M. Campbell, and I.H. Inoue: High intergranular critical currents in metallic MgB_2 superconductor. *Supercond. Sci. Technol.* **14**, L5 (2001).
8. H. Kotegawa, K. Ishida, Y. Kitaoka, T. Muranaka, and J. Akimitsu: Evidence for strong-coupling s-wave superconductivity in MgB_2: ^{11}B NMR study. *Phys. Rev. Lett.* **87**, 127001 (2001).
9. T. Takasaki, T. Ekino, T. Muranaka, H. Fujii, and J. Akimitsu: Multiple-gap structure of the binary superconductor MgB_2. *Physica C* **388–389**, 147 (2003).
10. S.X. Dou, S. Soltanian, W.K. Yeoh, and Y. Zhang: Effect of nano-particle doping on the upper critical field and flux pinning in MgB_2. *IEEE Trans. Appl. Supercond.* **15**, 3219 (2005).
11. H. Kumakura, H. Kitaguchi, A. Matsumoto, and H. Hatakeyama: Upper critical fields of powder-in-tube-processed MgB_2/Fe tape conductors. *Appl. Phys. Lett.* **84**, 3669 (2004).
12. M.D. Sumption, M. Bhatia, S.X. Dou, M. Rindfleisch, M. Tomsic, L. Arda, M. Ozdemir, Y. Hascicek, and E.W. Collings: Irreversibility field and flux pinning in MgB_2 with and without SiC additions. *Supercond. Sci. Technol.* **17**, 1180 (2004).
13. A. Yamamoto, J. Shimoyama, S. Ueda, Y. Katsura, S. Horii, and K. Kishio: Doping effects on critical current properties of MgB_2 bulks synthesized by modified powder-in-tube method. *IEEE Trans. Appl. Supercond.* **15**, 3292 (2005).
14. J. Wang, Y. Bugoslavsky, A. Berenov, L. Cowey, A.D. Caplin, L.F. Cohen, L.D. Cooley, X. Song, and D.C. Larbalestier: High critical current density and improved irreversibility field in bulk MgB_2 made by a scalable, nanoparticle addition route. *Appl. Phys. Lett.* **81**, 2026 (2002).
15. A. Matsumoto, H. Kumakura, H. Kitaguchi, and H. Hatakeyama: Effect of SiO_2 and SiC doping on the powder-in-tube processed MgB_2 tapes. *Supercond. Sci. Technol.* **16**, 926 (2003).
16. G.J. Xu, J.C. Grivel, A.B. Abrahamsen, and N.H. Andersen: Enhancement of the irreversibility field in bulk MgB_2 by TiO_2 nanoparticle addition. *Physica C* **406**, 95 (2004).
17. M. Gharaibeh, B.A. Albiss, I. Jumah, and I.M. Obaidat: Effective incorporation of nanoceria into polycrystalline MgB_2. *J. Appl. Phys.* **107**, 063908 (2010).
18. C. Yao, X. Zhang, D. Wang, Z. Cao, L. Wang, Y. Qi, C. Wang, Y. Ma, S. Awaji, and K. Watanabe: Doping effects of Nd_2O_3 on the superconducting properties of powder-in-tube MgB_2 tapes. *Supercond. Sci. Technol.* **24**, 055016 (2011).
19. J. Jiang, B.J. Senkowicz, D.C. Larbalestier, and E.E. Hellstrom: Influence of boron powder purification on the connectivity of bulk MgB_2. *Supercond. Sci. Technol.* **19**, L33 (2006).
20. X.Z. Liao, A.C. Serquis, Y.T. Zhu, J.Y. Huang, D.E. Peterson, F.M. Mueller, H.F. Xu: Controlling flux pinning precipitates during MgB_2 synthesis. *Appl. Phys. Lett.* **80**(23), 4398 (2002).
21. R.F. Klie, J.C. Idrobo, N.D. Browning, A. Serquis, Y.T. Zhu, X.Z. Liao, and F.M. Muelle: Observation of coherent oxide precipitates in polycrystalline MgB_2. *Appl. Phys. Lett.* **80**(21), 3970 (2002).

22. C.B. Eom, M.K. Lee, J.H. Choi, L.J. Belenky, X. Song, L.D. Cooley, M.T. Naus, S. Patnaik, J. Jiang, M. Rikel, A. Polyanskii, A. Gurevich, X.Y. Cai, S.D. Bu, S.E. Babcock, E.E. Hellstrom, D.C. Larbalestier, N. Rogado, K.A. Regan, M.A. Hayward, T. He, J.S. Slusky, K. Inumaru, M.K. Haas, R.J. Cava: High critical current density and enhanced irreversibility field in superconducting MgB_2 thin films. *Nature* **411**, 558 (2001).
23. C.H. Jiang, H. Hatakeyama, and H. Kumakura: Effect of nanometer MgO addition on the in situ PIT processed MgB_2/Fe tapes. *Physica C* **423**, 45 (2005).
24. M. Eisterer: Magnetic properties and critical currents of MgB_2. *Supercond. Sci. Technol.* **20**, R47 (2007).
25. D. Dew-Hughes: Flux pinning mechanisms in type II superconductors. *Philos. Mag.* **30**, 293 (1974).